

Dynamical yield criterion for granular matter from first principlesO. Coquand^{1,2,*} and M. Sperl^{1,3,†}¹*Institut für Materialphysik im Weltraum, Deutsches Zentrum für Luft- und Raumfahrt (DLR), 51170 Köln, Germany*²*Laboratoire de Modélisation Pluridisciplinaire et Simulations, Université de Perpignan Via Domitia, 52 avenue Paul Alduy, F-66860 Perpignan, France*³*Institut für Theoretische Physik, Universität zu Köln, 50937 Köln, Germany*

(Received 3 November 2023; accepted 13 February 2024; published 4 March 2024)

We investigate, using a recently developed model of liquid state theory describing the rheology of dense granular flows, how a yield stress appears in granular matter at the yielding transition. Our model allows us to predict an analytical equation of the corresponding dynamical yield surface, which is compared to the usual models of solid fracture. In particular, this yield surface interpolates between the typical failure behaviors of soft and hard materials. This work also underlines the central role played by the effective friction coefficient at the yielding transition.

DOI: [10.1103/PhysRevE.109.034901](https://doi.org/10.1103/PhysRevE.109.034901)**I. INTRODUCTION**

Understanding the way solid objects break is a question relevant to various areas of physics. At a fundamental level, the determination of the precise mechanism at the origin of solid failure, be it via elastoplastic models [1–6], statistical methods inspired from glassy physics [7,8], or modified elasticity theories [9–15], as well the still debated relationship between the brittle and ductile modes of failure [16–27] are very active fields of research. However, this topic is also ubiquitous in applied physics and engineering for the study of the failure of rocks, soils, and other geomaterials [28–35]; concrete [36–39]; or cellular materials [40]. A particularly successful approach consists in determining the yield surface of the solid, a curve that allows to determine whether a solid in a given state of stress will yield. Many different constructions of such an object have been proposed [41–51], but for amorphous solids, for which determining the yielding point from *ab initio* methods used in crystals [52] is not possible, nor has a generally accepted construction of a yield criterion has been determined yet.

In this paper, we propose a study of the yielding transition based not on a theory of the solid, but of the liquid state. More precisely, using a theory developed to describe the non-Newtonian features of granular liquid flows [53–59] in the limit of very low shear rates, we describe how an internal state of stress develops into the liquid as its behavior becomes more and more solid-like. Such a determination of a so-called *dynamical yield criterion* has previously been done for the study of colloidal suspensions close to the mode coupling glass transition [60]. Although there is no evidence suggesting a complete equivalence between the dynamical yield criterion determined when approaching the yielding transition from the liquid side and the yield criteria studied in triaxial tests

when breaking solids, it is reasonable to assume that some properties are preserved across the transition. To that extent, our work brings an original insight on the yielding problem with an approach, which, contrary to many failure models, is based on fundamental principles.

The reduction of our liquid state theory to an analytically solvable model, along the lines presented in previous works [58,59] allows us to derive an analytical expression of the yield surface for granular materials. This surface turns out to display interesting properties, such as the existence *a priori* of two continuously related fracture modes (a soft and a hard one). Furthermore, the solvability of the model allows us to present a critical analysis of some widely used yield criteria. Finally, we show that a definition of the effective friction coefficient from the symmetries of the stress tensor allows us to build a quantity which behaves very smoothly across the transition to the solid state, thereby pointing out a potentially crucial quantity to understand how solid order builds up in complex liquids.

II. INTRODUCTION TO FRACTURE

Our aim in this section is not to give a complete review of the theory of fracture in solids. We present some of the features of usual yield criteria which are relevant to the following [61]. For sake of clarity, we restrict ourselves to the most usual yield criteria, many more refined ones being simple variations around those.

The state of stress in a solid piece of material can be represented by a stress tensor σ , which can be further decomposed into irreducible representations of the SO(3) group into a diagonal part (spin 0 representation) and a traceless, deviatoric component (spin 2 representation):

$$\sigma = P \mathbb{I} + \sigma', \quad (1)$$

where $P = \text{Tr}(\sigma)/3$ is the pressure and $\text{Tr}(\sigma') = 0$. The same decomposition can be applied to the strain tensor ϵ . In particular, for elastic materials, the deviatoric parts of both tensors

*oliver.coquand@univ-perp.fr

†matthias.sperl@dlr.de

are related by $\sigma' = 2G\epsilon'$, which defines the shear modulus G of the solid. Since most of the following work concerns shear fracture, the other elastic moduli shall not be discussed.

Another useful representation of σ is given by its three eigenvalues (or principal stresses) σ_1 , σ_2 , and σ_3 , which do not depend on the basis used to represent the stress tensor. One can then define three invariants in the following way:

$$\begin{aligned} I_1 &= \sigma_1 + \sigma_2 + \sigma_3, \\ I_2 &= \sigma_1\sigma_2 + \sigma_2\sigma_3 + \sigma_3\sigma_1, \\ I_3 &= \sigma_1\sigma_2\sigma_3. \end{aligned} \quad (2)$$

Similar definitions can be used to define the invariants J_2 and J_3 from σ' .

Most of the yield criteria can be understood in terms of an effective friction coefficient. This coefficient can be defined in the following ways.

Definition 1. In a solid, the effective friction coefficient μ compares the strength of the spin 0 and the spin 2 components of the stress tensor. It can then be expressed as $\mu = \sigma_0/P$, where the shear stress is $\sigma_0 = \sigma : \epsilon' / |\epsilon'|$, “:” denotes a full tensor contraction, and the norm of the deviatoric strain is $|\epsilon'|^2 = 2\epsilon' : \epsilon'$.

Definition 2. For two pieces of a broken solid to be able to glide onto one another, they have to overcome the solid friction between the two blocks, as defined by Coulomb’s law. The effective friction coefficient μ of the solid is defined as the ratio of tangential to normal stress on a given plane that has to be overcome for the solid to break along that plane. Both definitions are related to one another, although not equivalent [33].

Let us suppose that a piece of solid breaks as soon as the elastic energy E'_{el} accumulated due to the deviatoric strain exceeds a certain proportion of the isotropic part of the elastic energy $E'_{el} \propto P$. The first energy can be expressed as $E'_{el} = \sigma' : \epsilon' / 2 = J_2 / 4G$. The corresponding shear stress is $\sigma_0 = \sqrt{J_2} / 2G$. Finally, using the definition 1 of the effective friction coefficient, the material yields when μ exceeds a characteristic value of the material, μ_{DP} , which defines the Drucker-Prager yield criterion [41]. It can also be written in terms of invariants as $J_1^2 / I_2 = C_{DP}$, where C_{DP} is a constant.

The main advantage of definition 1 is that it only depends on the symmetries of the stress tensor. However, determining ϵ' in a given experimental situation can be challenging. As a result, many yield criteria are based on the second definition of μ . In that case, the main difficulty is to determine the fracture plane on which the tangential and normal stresses must be compared.

One of the simplest way to proceed is to assume that the fracture will take place in one of the principal planes. In that case, the problem reduces to three two-dimensional problems which are very easy to solve. The material yields as soon as $\mu \geq \mu_{MC}$ on one of the three principal planes, which defines the Mohr-Coulomb yield criterion.

This approach can be refined further by approximating the fracture plane by the so-called *spatially mobilized plane* [45,48], which is a clever interpolation between the three principal planes. More precisely, it is defined as the unique plane, which projections onto the three principal planes gives back the Mohr-Coulomb problem [45]. By removing the

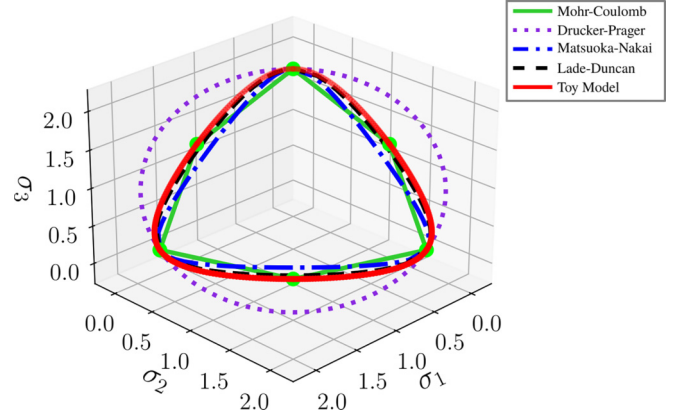


FIG. 1. Comparison of the different yield criteria presented in this paper. The big green dots are the points used to adjust the constants of the Mohr-Coulomb criterion (as well as their images by rotation of angle $2\pi/3$). The constants of the three other criteria are adjusted on the upper apex.

possibility that the fracture plane evolves discontinuously from one principal plane into another, it provides a much smoother version of the Mohr-Coulomb yield surface (see Fig. 1). In terms of invariants, this can be written $C_{MN} = I_2 I_1 / I_3$, where C_{MN} is a constant.

Finally, another popular smooth version of the Mohr-Coulomb criterion is the Lade-Duncan yield criterion [43]. Its geometrical interpretation is not as straightforward as the previous ones, but it was recently showed [51] that it can be understood as a correction to the Matsuoka-Nakai criterion taking into account subleading dependence in J_2/P . By cumulating the expressions of the Drucker-Prager and Matsuoka-Nakai constants, a new quantity $C_{LD} = C_{MN} C_{DP} = I_3^3 / I_3$ can be constructed. The Lade-Duncan criterion can then be defined by requiring that C_{LD} , rather than C_{MN} and C_{DP} separately, is constant [51]. The corresponding modification in terms of effective friction coefficient μ_{LD} is given in [51].

A comparison of the different yield criteria is presented on Fig. 1, which presents a cut of the yield surface along one of the deviatoric planes (planes at constant pressure). Remarkably, the Drucker-Prager yield surface is much more isotropic than all the other ones. This can be related to the absence of dependence in I_3 , which confers it a higher degree of symmetry. The more triangular shape of the three other criteria, on the other hand, can be related to the nonzero value of the effective friction coefficient [62], thereby illustrating the inequivalence between definitions 1 and 2 given above (μ is obviously also nonzero for the Drucker-Prager yield surface in Fig. 1).

All in all, the most usual yield criteria used for studying solid fracture can be captured in terms of an effective friction coefficient μ , which should not exceed a given value for solid order to be preserved.

III. RESULTS

A. Yielding transition from the liquid state

The model we present in this paper is based on a simplification of the granular integration through transients (GITT)

formalism. For more details about this model, the reader is referred to the more detailed previous publications on the subject [53–59], as well as the Appendix. This formalism is based on the so-called integration through transients (ITT) formalism [60,63–65], which allows to compute statistical averages in a sheared fluid by relating them to averages computed in a quiescent state where no shear is applied. We can therefore decompose the stress tensor as: $\sigma = \sigma^{(0)} + \Delta\sigma$, where $\sigma^{(0)} = P_0\mathbb{I}$ because the quiescent fluid is not sheared and $\Delta\sigma$ contains all the corrections depending on the shear rate $\dot{\gamma}$. The pressure P_0 can be computed for a fluid at equilibrium [57], but can also include an isotropic component imposed by the environment in many situations relevant to geophysics problems, and is thus left unspecified here. In our model, P_0 does not couple with the correction $\Delta\sigma$.

The stress correction $\Delta\sigma$ can also be written in a form similar to Eq. (1):

$$\Delta\sigma = \Delta P\mathbb{I} + \eta D, \quad (3)$$

where ΔP is the correction to the pressure due to shear, η is the viscosity of the liquid, and $D_{ij} = \kappa_{ij} + \kappa_{ji}$ is the symmetrized flow matrix, $\kappa = \nabla\mathbf{v}$ being the velocity gradient. In this work, we restrict ourselves to incompressible flows for which $\text{Tr}(\kappa) = 0$. Note that the dilation of the granular packing under shear can be safely neglected here since we work at a macroscopic scale much bigger than that of the individual granular particle.

The GITT equations allow to relate $\Delta\sigma$ to κ via a viscosity matrix Λ through $\Delta\sigma_{ab} = \Lambda_{abij}\kappa_{ij}$. In this formalism, the components of Λ can be written explicitly as integrals over time and wave vectors of the density correlation function $\langle\rho_k(t)\rho_{-k}(0)\rangle$ [59]. Our toy model consists in neglecting the wave vector dependences which play a subleading role (details in the Appendix and [58,59]). In that case, Λ reduces to integrals over time of the products of the Finger tensor, which contains information about the deformation of the system, and the density correlation function (see the Appendix for a detailed derivation). Then, the density correlation function is reduced to the following expression:

$$\langle\rho_k(t)\rho_{-k}(0)\rangle \propto e^{-t/t_\Gamma} e^{-\dot{\gamma}^2 t^2 / 2\gamma_c^2}. \quad (4)$$

The first factor accounts for the internal dynamics of the liquid, with a typical timescale t_Γ . As the behavior of the liquid becomes more and more solid-like, t_Γ becomes very large, mostly due to the cage effect: in dense liquids, the particles' ability to move tends to be reduced by their neighbors. The second factor is a screening factor accounting for the effect of advection: the applied stress tends to force particles to move and facilitates the escape from the cages. This screening is characterized by a strain scale γ_c , which is a constant of the material describing its compliance to external stresses. Despite its simplicity, the reduction of the contribution to the stress tensor of the particle's dynamics by equations like Eq. (4) has proven to provide rather accurate constitutive equations for dense granular liquids [58,59].

The final element of our toy model is the sampling of possible flow geometries. First, we restrict ourselves to the basis in which σ is diagonal, so that κ is also diagonal. Then, we map the space of traceless diagonal matrices by the following

two parameters family of reduced flow matrices

$$\bar{\kappa} = \begin{pmatrix} A_2 & 0 & 0 \\ 0 & -A_2\left(\frac{1-A_1}{2}\right) & 0 \\ 0 & 0 & -A_2\left(\frac{1+A_1}{2}\right) \end{pmatrix}, \quad (5)$$

where (A_1, A_2) defines the flow geometry and $\kappa = \bar{\kappa}\dot{\gamma}$. For this family of flows, and in the case of stationary flows, the toy model integrals giving the components of Λ can be evaluated exactly. Finally, we can examine the limit $\dot{\gamma} \rightarrow 0$, which allows two distinct behaviors. For low packing fraction systems, the ITT correction vanishes with $\dot{\gamma}$, the system remains a liquid. For denser systems, a nontrivial yield stress develops in this limit, which signals the onset of solid-like behavior. The corrections to the eigenvalues of the stress tensor predicted by the toy model in the latter case can then be expressed as follows:

$$\begin{aligned} \Delta\sigma_1 &= \frac{S_0 + S_1}{2} \sqrt{\pi} [\mathcal{F}(\bar{\kappa}_1\gamma_c) + \mathcal{F}(\bar{\kappa}_2\gamma_c) + \mathcal{F}(\bar{\kappa}_3\gamma_c)] \\ &\quad + S_1 \sqrt{\pi} \mathcal{F}(\bar{\kappa}_1\gamma_c), \\ \Delta\sigma_2 &= \frac{S_0 + S_1}{2} \sqrt{\pi} [\mathcal{F}(\bar{\kappa}_1\gamma_c) + \mathcal{F}(\bar{\kappa}_2\gamma_c) + \mathcal{F}(\bar{\kappa}_3\gamma_c)] \\ &\quad + S_1 \sqrt{\pi} \mathcal{F}(\bar{\kappa}_2\gamma_c), \\ \Delta\sigma_3 &= \frac{S_0 + S_1}{2} \sqrt{\pi} [\mathcal{F}(\bar{\kappa}_1\gamma_c) + \mathcal{F}(\bar{\kappa}_2\gamma_c) + \mathcal{F}(\bar{\kappa}_3\gamma_c)] \\ &\quad + S_1 \sqrt{\pi} \mathcal{F}(\bar{\kappa}_3\gamma_c), \end{aligned} \quad (6)$$

where $\mathcal{F}(x) = x e^{x^2} \text{erfc}(-x)$, and S_0 and S_1 are constants from the toy model giving the typical strength of the yield stress developing in the liquid (they have very little influence on the geometry of the yield surface).

The yield surface equation Eqs. (6) is quite remarkable. Indeed, it was shown in [50] that all the usual yield criteria defined above can be expressed as roots of a polynomial equation of degree three. Here, to the contrary, the eigenvalues of the stress tensor, defined from the function \mathcal{F} are highly nonpolynomial, which make Eqs. (6) quite unique to the best of our knowledge. As shown in the Appendix, the Drucker-Prager criterion can be recovered from a $A_2\gamma_c \ll 1$ expansion of Eqs. (6), but the relation to the other usual yield criteria is more involved [66].

B. Geometry of the yield surface

In Fig. 2, we represent the surface Eqs. (6) in various deviatoric planes, corresponding to various values of I_1 . More precisely, fixing a pressure amounts to fixing the pressure correction ΔP , which is our control parameter along the hydrostatic axis since P_0 does not couple to the shear corrections to the stress. All quantities are dimensionless, the global scale of the axis in physical units being fixed by the value of the parameters S_0 and S_1 .

The yield surface presents two qualitatively different behaviors from which we identify two fracture modes: For $\Delta P \simeq S_0, S_1$, the shape of the yield surface cuts is triangular, similar to that of Fig. 1, which corresponds to the typical shape observed in the failure of sedimentary rocks and soils captured by yield criteria from the family of

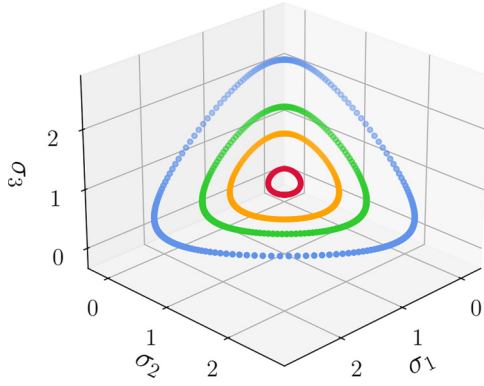


FIG. 2. Cuts of the toy model yield surface along the deviatoric plane for various values of ΔP . The parameters are $S_0 = S_1 = 1$, $\gamma_c = 0.4$, $\Delta P = 0.05$ (red), $\Delta P = 0.5$ (orange), $\Delta P = 1$ (green), and $\Delta P = 2$ (blue).

Mohr-Coulomb–Matsuoka-Nakai–Lade-Duncan, we call this mode of fracture *hard*; For $\Delta P \ll S_0, S_1$ on the other hand, the yield surface cuts become isotropic, and the yield surface has a Drucker-Prager like shape, we call this fracture mode the *soft* mode. This can be used to classify material according to their preferred mode of fracture, softer materials being the ones for which the shear induced pressure component of the stress is small compared to the typical scale of stress involved.

The soft fracture mode was already described in the yielding of soft colloids close to the mode coupling glass transition [60]. This picture fits well our current framework: close to the mode coupling glass transition, the shear correction to the pressure is rather mild compared to the other stress scales in the system. One of the main nontrivial additional outcomes of our model is that this fracture mode is only observed under certain conditions (more precisely $A_2\gamma_c \ll 1$, see the Appendix for details), and can be continuously transformed into a hard type of fracture by changing the conditions of fracture.

Coming back to the physical picture presented before, the soft fracture mode corresponds to materials where the primary mechanism of fracture is the excess of accumulated deviatoric energy compared to the isotropic elastic energy. As $\Delta P/S_0$ increases, the stress becomes more and more localized in specific regions inside the material, which is represented by the transition to the hard fracture mode. In the limit of large excess pressure ΔP , the yield surface resembles that obtained by identification of the spatially mobilized plane, where the stress becomes asymptotically localized in a two-dimensional manifold.

There are a number of reasons though why this transition between both fracture modes could not be observed experimentally. (i) While our model allows us to explore the variations of the yield surface with respect to any value of ΔP , there is no guarantee that there exists an experimental protocol which allows to explore such a region for a given material. Indeed, ΔP is itself a function of the applied shear stress. (ii) Our model so far only includes shear failure, but it is expected that adding the possibilities of dilation and compression failure puts material-dependent boundaries on

the hydrostatic axis, which may prevent it from exploring the full variation of the yield surface geometry.

Finally, the analytical expression of the yield surface Eqs. (6) allows us to analyze the performance of other yield criteria in various deviatoric planes. The results are displayed in Figs. 5–7 in the Appendix. While unsurprisingly the Drucker-Prager criterion performs all the best that ΔP is small, there is no such monotonous behavior for the precision of the Matsuoka-Nakai and Lade-Duncan criteria. It can be noted, though, that those later two perform all the best that the pressure P_0 is large.

C. Effective friction coefficient

We discussed in the first section how all usual yield criteria can be expressed in terms of an effective friction coefficient. Effective friction coefficients can also be defined for complex liquids. It is even a crucial quantity in the context of the study of granular liquids for which it has been shown that the dependence of μ on the shear rate is largely universal [67–69], and provides a useful tool to relate the rheology of granular liquids and granular suspensions [58,70–73].

Since the definition of a fracture plane is not appropriate for liquids, μ is naturally defined from the symmetries of the stress tensor, like in definition 1 above. More precisely, the spin 0 component of the stress tensor of the liquid is the total pressure $P = P_0 + \Delta P$, and its deviatoric component defines a shear stress σ_0^l as $\sigma_0^l = \sigma : \kappa / |\kappa|$ [59], with $|\kappa|^2 = D : D/2$. This defines an effective friction coefficient as $\mu = \sigma_0^l/P$.

In a Newtonian liquid, the deviatoric stress is $\sigma' = \eta D$ [from Eq. (3)]. Because η is a constant, this component of the stress vanishes in the limit $\dot{\gamma} \rightarrow 0$. For complex liquids however, $\sigma' = \eta(\dot{\gamma})D$. Hence, provided that $\eta \sim 1/\dot{\gamma}$ in the limit of low shear rates, this term survives and solid-like behavior builds up. All in all, analyzing the deviatoric component of the stress tensor in the limit of low shear rates makes the connection between the liquid and solid definitions of the shear stress σ_0 . However, both definitions of σ_0 are not necessarily equivalent to one another. Indeed, outside the regime of small strains, the deviatoric part of the deformation tensor is not proportional to the symmetrized velocity gradient D [74].

Within our model, it is possible to identify from the stress equations (6) the contribution of the strain tensor (see the details in the Appendix), and thus to get access to its deviatoric component. Hence, we can compare σ_0^l , computed from the velocity gradient, to $\sigma_0^s = \sigma : \epsilon' / |\epsilon'|$, computed from the solid-like expression of the stress tensor Eq. (1). The results are displayed in Fig. 3 for various values of ΔP [75]. We can see that, although some variation is indeed present, both definitions yield very compatible numerical values. Consequently, μ defined from the ratio of the spin 2 and spin 0 component of the stress tensor behaves very smoothly across the liquid-solid transition, and therefore appears to be a particularly interesting quantity to study the onset of solid order in freezing liquids under shear.

Finally, our model allows us to perform a more in-depth analysis of the behavior of μ in a given deviatoric plane (data in the Appendix). First, μ is not constant along those planes, although relative variations are quite small. Provided that our

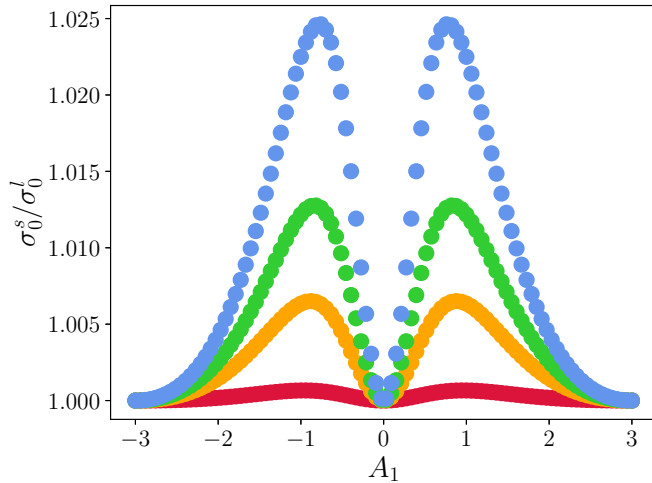


FIG. 3. Comparison of the definition of the shear stress from the solid state stress tensor σ_0^s and from the liquid state stress tensor σ_0^l . The data are represented as a function of A_1 , the variation of which on the presented scale corresponds to a sector of the $2\pi/3$ Lode angle. The parameters are $S_0 = S_1 = 1$, $\gamma_c = 0.4$, $\Delta P = 0.05$ (red), $\Delta P = 0.5$ (orange), $\Delta P = 1$ (green), and $\Delta P = 2$ (blue).

model still holds for solid fracture, this means that a way to improve the existing yield criteria could be to allow for a such a deviation to the constant value, a feature which is present in none of the solid yield criteria presented in the first section of the paper. Then, the relative variation of μ with the Lode angle are all the bigger that the fracture mode becomes harder. Given that, as shown above, the hard fracture mode corresponds to cases very well described by criteria based on definition 2 of the effective friction coefficient, this raises the question of a possible transition between the two definitions as the isotropic stress ΔP caused by shear becomes more and more comparable to the intrinsic stress scale of the material fixed by S_0 and S_1 : the definition of μ from the liquid stress tensor (3) accounts for the build up of solid-like behavior as the liquid's behavior gets less and less Newtonian, then for the soft type of solid fracture mode, the approximation of μ , set by definition 1, by a constant is quite accurate, but deteriorates as the fracture mode becomes harder, where, given the good performance of yield criteria based on definition 2, a constant μ based on definition 2 could still be observed. Furthermore, since the value of μ on the fracture plane is determined by the value of the yield criterion constant [51], we can also study the variations of μ from definition 2 within our toy model. Notably, there seems to be a regime where $P_0 \simeq 1$ (in units of S_0, S_1) where the relative variation of μ_{MN} and μ_{LD} is suppressed at best. However, since the value of P_0 , playing a central role in that case, is not prescribed by our model, quantitative comparison to the relative variations with definition 1 is not possible.

IV. CONCLUSION

All in all, we built an analytically solvable toy model that allows us to predict the shape of the dynamical yield surface of soft materials and granular matter. Importantly, our yield

criterion is based on fundamental equations of liquid state theory rather than some phenomenological rule. The study of this model allowed us in particular to highlight the role of the effective friction coefficient μ that appears to be a particularly interesting quantity to relate the properties of the liquid close to the yielding transition and those of the corresponding solid state. It also predicted a nontrivial shape for the yield surface that smoothly interpolates between known shapes for soft and hard materials.

The picture emerging from this study raises a number of questions. (i) How is the yield surface shape modified by the addition of the compression and dilation fracture modes? This question can be answered by extending our toy model to compressible flows, in which case the liquid-like stress tensor provides both a shear and a bulk modulus in the limit $\dot{\gamma} \rightarrow 0$. (ii) Is there a meaningful transition between definition 1 and 2 of the effective friction coefficient as the solid becomes harder? Would an extension of our model to account for shear banding highlight some mechanisms of this transition? (iii) What is the influence of the dependence of μ on the Lode angle, and thus on the stress geometry on the definition of the jamming transition, where μ is supposed to reach a fixed value through a power-law evolution controlled by a critical exponent?

ACKNOWLEDGMENTS

This work was funded by the Deutscher Akademischer Austauschdienst (DAAD). We warmly thank Th. Voigtmann for stimulating discussions and helpful suggestions. We thank O. Pouliquen for enlightening discussions. We also thank Till Kranz for his useful comments on the manuscript.

APPENDIX A: GITT EQUATIONS AND TOY MODELS

In this Appendix, we quickly review the foundations of the toy model used in the main paper.

1. Dynamics

The dynamics of the particles is accounted for through the evolution of the dynamical structure factor $\Phi_q(t) = \langle \rho_q(t) \rho_{-q}(0) \rangle / S_q$, where ρ_q is the density operator in Fourier space, and $S_q = \langle \rho_q(0) \rho_{-q}(0) \rangle$ is the static structure factor. Its evolution with time is given by a mode coupling equation of motion, which has the following schematic structure:

$$\ddot{\Phi}_q(t) + \nu_q \dot{\Phi}_q(t) + \Omega_q^2 \Phi_q(t) + \Omega_q^2 \int_0^t d\tau m_q(t, \tau) \dot{\Phi}_q(\tau) = 0, \quad (\text{A1})$$

where ν_q and Ω_q are characteristic frequencies, and m_q is called the memory kernel. The explicit expression of those terms is not needed for the following argument. The qualitative behavior of the solutions to Eq. (A1) is as follows. When the memory term is small enough, Eq. (A1) reduces to a linear second-order differential equation whose solutions have a decaying exponential envelope. When the memory term is large, typical solutions saturate to a finite plateau value at large time, signaling the onset of solid behavior.

There are no analytical expression that captures well the global expression of the solutions to Eq. (A1), hence building analytically solvable models require to do some approximations. A finer way to capture the behavior of $\Phi_q(t)$ is to use the Vineyard approximation, which decomposes it in a product of static structure factor and self correlation function, and then use an exponential ansatz for the latter term:

$$\Phi_q(t) \simeq S_q e^{-q^2 \langle \Delta r^2(t) \rangle}, \quad (\text{A2})$$

where $\langle \Delta r^2(t) \rangle$ is the mean squared displacement. It is not difficult to check that the usual evolutions of $\langle \Delta r^2(t) \rangle$ yields the expected qualitative phenomenology: for simple liquids, the large time behavior of $\langle \Delta r^2(t) \rangle$ is given by the law of diffusion $\langle \Delta r^2(t) \rangle \sim t$, which corresponds to the case of negligible memory effects with an exponential envelope of the decay, whereas in a solid, particles acquire a well-defined mean position, $\langle \Delta r^2(t) \rangle$ reaches a finite limit value, and $\Phi_q(t)$ evaluated from Eq. (A2) does indeed saturate.

From this qualitative analysis, we draw two main conclusions: (i) the wave-vector dependence is irrelevant to understand the time evolution of $\Phi_q(t)$, at least in a lowest-order approximation (notice that the same type of argument is used when using schematic mode coupling models, such as those used in [60,64]) and (ii) the whole complexity of Eq. (A1) can be captured in a very crude way by a simple exponential ansatz $\Phi_q(t) \simeq \exp(-\Gamma t)$, where $\Gamma = 1/t_\Gamma$ is the structural relaxation rate. Of course, we do not pretend to capture all the mode coupling physics by this very simple ansatz, but it already captures the most relevant physical phenomena at play (in that case the slow down of the dynamics due to the structural relaxations in dense systems), and with only minor modifications [namely, the addition of a second step in the decay of $\Phi_q(t)$], it provides a convincing model of the rheology of dense granular flows [57,58], allowing, for example, to recover the universal $\mu(\mathcal{I})$ of granular rheology.

Finally, when going to the case of a sheared complex fluid, the effect of the advection of particles by the external shear stress has to be taken into account. Within our approach, this is done by evaluating the dynamical structure factor Φ at the wave vector $q(t)$ advected by the shear flow, rather than simply q . Equation (A2) then becomes

$$\Phi_{q(t)}(t) \simeq S_q e^{-q(t)^2 \langle \Delta r^2(t) \rangle}, \quad (\text{A3})$$

where $\mathbf{q}(t) = F(t) \cdot \mathbf{q}$, and $F(t) = \exp(-\kappa t)$ is the deformation gradient [74]. For simple shear flows, κ is nilpotent, and $F(t) = \mathbb{I} - \kappa t$ exactly, but this relationship is not valid anymore for more general flows. Since $q(t)$ is typically ever increasing, this provides a new channel of decay for Φ : Even when the packing fraction is so dense that $\langle \Delta r^2(t) \rangle$ should saturate to a constant value, the $q(t)^2$ factor in the exponential guarantees that Φ decays to zero. Physically, this corresponds to the fact that the motion imposed by the advection of particles by the applied shear stress is strong enough to break the cages, so that the systems always flow on some timescale.

Because our toy model is so far independent of q , it is blind to the change of q to $q(t)$. To account for advection, we therefore add a screening term that introduces the advection

channel of decay. Guided by results in the case of simple shear flows [58], and the useful properties of Gaussian functions, we define the screening factor as $\exp(-\dot{\gamma}^2 t^2 / 2\gamma_c^2)$, where γ_c is a typical strain scale. As a matter of fact, the precise form of the screening is not really important to grasp the main properties of the rheology, [60] for example, use a Lorentzian profile with similar results.

All in all, at the level of the dynamics, our toy model can be summarized by $\Phi_{q(t)}(t) \simeq \Phi_{\text{toy}}(t) = \exp(-\Gamma t) \exp(-\dot{\gamma}^2 t^2 / 2\gamma_c^2)$. It has two parameters: the structural relaxation rate Γ and the strain scale γ_c .

2. Link to the rheology

The dynamics evolution is then linked to the rheology by use of the integration through transients (ITT) formula [56,60,63–65]. Using this approach, the shear correction to the stress tensor is expressed as an integral over the time evolution of a fictitious reference state, where the fluid is not sheared

$$\Delta \sigma_{\alpha\beta} = \frac{1}{2T} \int_0^{+\infty} dt \int_k \mathcal{V}_{k(-t)}^\sigma \Phi_{k(-t)}(t)^2 \mathcal{W}_{k,\alpha\beta}^\sigma, \quad (\text{A4})$$

where the mode coupling vertices $\mathcal{V}_k^\sigma = \sum \kappa_{\theta\omega} \mathcal{V}_{k,\theta\omega}^\sigma$ and $\mathcal{W}_{k,\alpha\beta}^\sigma$ are introduced, and $\int_k = \int d^3k / (2\pi)^3$. Without going into the details, the vertices can be expressed as

$$\begin{aligned} \mathcal{V}_{k,\alpha\beta}^\sigma &= \hat{k}_\alpha \hat{k}_\beta k \Delta \sigma + \delta_{\alpha\beta} \sigma_\perp, \\ \mathcal{W}_{k,\alpha\beta}^\sigma &= \frac{1 + \varepsilon}{2S_k^2} [\hat{k}_\alpha \hat{k}_\beta k \Delta \sigma + \delta_{\alpha\beta} \sigma_\perp], \end{aligned} \quad (\text{A5})$$

as a function of the following reduced scalars:

$$\begin{aligned} \sigma_\perp &= T [S_k - S_k^2], \\ \Delta \sigma &= -T S_k', \end{aligned} \quad (\text{A6})$$

the restitution coefficient of the granular particles ε , $S_k' = dS_k/dk$, and the normalized wave vector components \hat{k}_α . Note that the above formula can be applied to colloidal suspensions by taking the elastic limit $\varepsilon \rightarrow 1$.

Given that we defined above a procedure of approximation of the $\Phi_{k(-t)}^2(t)$ term, the next step is to reduce the tensorial structure of the mode coupling vertices. Factoring out the $\kappa_{\theta\omega}$ term embedded in the vertex \mathcal{V}_k^σ , our integral becomes a tensor of rank four corresponding to the viscosity tensor $\Lambda_{\alpha\beta\theta\omega}$. The vertex product is then developed:

$$\begin{aligned} \mathcal{V}_{k,\theta\omega}^\sigma \mathcal{W}_{k,\alpha\beta}^\sigma &\propto \delta_{\alpha\beta} \delta_{\theta\omega} \sigma_\perp^2 + \delta_{\theta\omega} \hat{k}_\alpha \hat{k}_\beta k \sigma_\perp \Delta \sigma \\ &\quad + \delta_{\alpha\beta} \hat{k}_\theta(-t) \hat{k}_\omega(-t) k(-t) \sigma_\perp \Delta \sigma \\ &\quad + \hat{k}_\alpha \hat{k}_\beta \hat{k}_\theta(-t) \hat{k}_\omega(-t) k k(-t) \Delta \sigma^2. \end{aligned} \quad (\text{A7})$$

Then, we use the deformation gradient $F(t)$ introduced above to extract the remaining time dependence carried by the wave vectors by $\hat{k}_\alpha(t) = F_{\alpha v}(t) \hat{k}_v$. The remaining time-independent wave-vector component being the only nonisotropic terms, the spherical part of the k integral can be performed. We use the following formula:

$$\int_k k_i k_j f(k^2) = \frac{\delta_{ij}}{3} \int_k f(k^2), \quad (\text{A8})$$

and

$$\int_k k_i k_j k_a k_b f(k^2) = \frac{X_{ijab}}{15} \int_k f(k^2), \quad (\text{A9})$$

where we defined the fully symmetrized product of kronecker symbols as

$$X_{ijab} = \delta_{ij}\delta_{ab} + \delta_{ia}\delta_{jb} + \delta_{ib}\delta_{ja}. \quad (\text{A10})$$

Finally, $\Phi_{k(-t)}(t)$ is replaced by $\Phi_{\text{toy}}(t)$, and the remaining integral over the norm of k reduces to a constant prefactor.

After all the above steps are performed, the viscosity tensor can be decomposed along the three following terms:

$$\begin{aligned} \mathcal{B}_{\alpha\beta\theta\omega}^{\text{comp}} &= \delta_{\alpha\beta}\delta_{\theta\omega} \int_0^{+\infty} dt \Phi_{\text{toy}}^2(t), \\ \mathcal{B}_{\alpha\beta\theta\omega}^0 &= \delta_{\alpha\beta} \int_0^{+\infty} dt \Phi_{\text{toy}}^2(t) [\delta_{\theta\omega} + F_{v\theta}(-t)F_{v\omega}(-t)], \\ \mathcal{B}_{\alpha\beta\theta\omega}^1 &= X_{\alpha\beta\nu\iota} \int_0^{+\infty} dt \Phi_{\text{toy}}^2(t) F_{v\theta}(-t)F_{\iota\omega}(-t). \end{aligned} \quad (\text{A11})$$

In the above formula, $\mathcal{B}^{\text{comp}}$ comes from the σ_{\perp}^2 term. It never contributes to $\Delta\sigma$ for incompressible flows. \mathcal{B}^0 comes from the $\sigma_{\perp}\Delta\sigma$ term in Eq. (A7), the constant prefactor defines S_0 . It includes both the effect of restitution coefficient and the remnants of the k integral. The first term in the bracket only contributes in the case of compressible flows. The second term is the Finger tensor, the inverse of the right Cauchy-Green deformation tensor. Lastly, \mathcal{B}^1 comes from the $\Delta\sigma^2$ term in Eq. (A7) and its prefactor defines S_1 . Thus, in the case of incompressible flows, two scaling constants (S_0 and S_1) are needed, and all the contributions to Λ have the form of a time integral of the product $\Phi_{\text{toy}}(t)$ and two deformation gradients, with varying types of tensor contractions.

For the last step, let us place ourselves in the basis in which the flow matrix is diagonal. In that case, it is possible to show that the remaining contributions in Eqs. (A11) only involve one component of κ at a time, say κ_{jj} . A typical term will hence have the following form:

$$\begin{aligned} \kappa_{jj} \int_0^{+\infty} dt \exp\left(-2\Gamma t - \frac{\dot{\gamma}^2 t^2}{\gamma_c^2} + \kappa_{jj} t\right) \\ = \frac{\sqrt{\pi}}{2} \bar{\kappa}_{jj} \exp\left[\gamma_c^2 (\bar{\kappa}_{jj} + \Gamma/\dot{\gamma})^2\right] \text{erfc}\left[\gamma_c (\bar{\kappa}_{jj} + \Gamma/\dot{\gamma})\right]. \end{aligned} \quad (\text{A12})$$

Finally, our study is restricted to the study of dense granular liquids and suspensions, close to the yielding transition, which Weissenberg numbers Wi are very large, hence $\Gamma \ll \dot{\gamma}$, so that Eqs. (6) is recovered. Note that in the mode coupling paradigm, such systems are characterized by $\Gamma = 0$ because they would be solid if the system were not sheared. However, a weaker version of the argument is needed here: we only use the fact that $Wi \gg 1$. This corresponds to taking a limit $\dot{\gamma} \rightarrow 0$ under the constraint that $\Gamma \ll \dot{\gamma}$.

APPENDIX B: DRUCKER-PRAGER LIMIT

Let us discuss the limit of small ΔP . The value of ΔP can be deduced from Eqs. (6), and depends mainly on the behavior

of the function \mathcal{F} . Hereafter are some of its basic properties:

$$\begin{aligned} \lim_{x \rightarrow +\infty} \mathcal{F}(x) &= +\infty, \\ \lim_{x \rightarrow -\infty} \mathcal{F}(x) &= -\frac{1}{\sqrt{\pi}}. \end{aligned} \quad (\text{B1})$$

Then, the typical size of the argument of \mathcal{F} in Eqs. (6) is set by the combination $A_2\gamma_c$, A_1 fixing the relationship between the different components of κ [see Eq. (5)]. This combination contains both information of the strength of the shear flow, through A_2 , and the material's response, through γ_c . Because of Eq. (B1), and since $\text{Tr}(\kappa) = 0$, which ensures that at least one of its components is positive, if $A_2\gamma_c \gg 1$, ΔP is large. Consequently, the regime of small ΔP correspond to small or moderate values of $A_2\gamma_c$, which can be explored by an expansion in powers of $A_2\gamma_c$.

The expansion of \mathcal{F} around $x = 0$ is as follows:

$$\mathcal{F}(x) = x + \frac{2}{\sqrt{\pi}} x^2 + O(x^3). \quad (\text{B2})$$

Because $\text{Tr}(\kappa) = 0$, the first-order term in the expression of ΔP vanishes, leaving at leading order

$$\Delta P = I_1 - P_0 = \frac{(3S_0 + 5S_1)(3 + A_1^2)}{2} A_2^2 \gamma_c^2 + O(A_2^3 \gamma_c^3). \quad (\text{B3})$$

Since I_1 and P_0 are parameters of our model, the above relationship truncated at this order allows us to compute A_1 as a function of A_2 , and the parameters of the model on a given deviatoric plane.

The corresponding geometry of the yield surface can be deduced by studying the evolution of the stress tensor invariants. For example, applying the same expansion

$$J_2 = S_1^2 \pi \frac{3 + A_1^2}{2} A_2^2 \gamma_c^2 + O(A_2^3 \gamma_c^3), \quad (\text{B4})$$

so that combining it with Eq. (B3) yields

$$\frac{J_2}{I_1^2} = \frac{S_1^2 \pi}{2} \frac{I_1 - P_0}{(3S_0 + 5S_1)I_1^2} + O(A_2 \gamma_c). \quad (\text{B5})$$

This formula can be read as follows: (i) the cuts of the yield surface in a given deviatoric plane are circles and (ii) their radius is all the smaller that $\Delta P/(3S_0 + 5S_1)$ is small. It is the behavior of the Drucker-Prager yield surface. Such behavior is indeed observed with the yield surface of Eqs. (6), as can be seen on Fig. 4. As $A_2\gamma_c$ gets closer to 1, $\Delta P/(3S_0 + 5S_1)$ does also and the yield surface cuts become less and less isotropic.

Interestingly, the fact that the expression of the yield surface is known analytically also means that we can study the behavior of the constants associated with the other usual yield criteria in the same limit, namely the Drucker-Prager, Matsuoka-Nakai, and Lade-Duncan ones.

Let us first have a look at the Drucker-Prager constant $C_{\text{DP}} = I_1^2/I_2$. To have an idea of its typical values, it is instructive to have a look at the value of J_2 at the point of Lode angle equal to 0, which in our conventions corresponds to the uniaxial extension flow $\bar{\kappa}_{xx} = 1$, $\bar{\kappa}_{yy} = -1/2$, $\bar{\kappa}_{zz} = -1/2$. Indeed, this point is generally used to adjust the constants of various yield criteria since it corresponds to the point of maximum J_2 , or, said otherwise, the point furthest to the hydrostatic axis

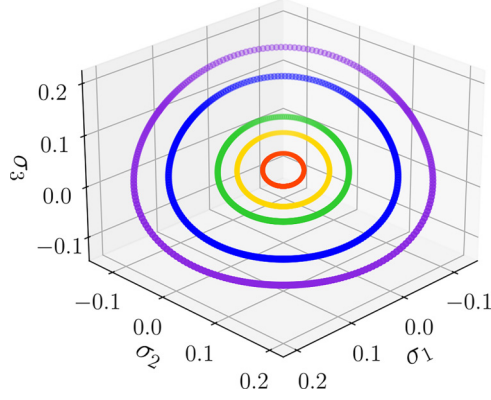


FIG. 4. Toy model yield surface for $\Delta P \ll S_0, S_1$. The parameters are $S_0 = S_1 = 1$, $\gamma_c = 0.4$, $\Delta P = 0.001$ (orange), $\Delta P = 0.005$ (yellow), $\Delta P = 0.01$ (green), $\Delta P = 0.03$ (blue), and $\Delta P = 0.05$ (violet).

$\sigma_1 = \sigma_2 = \sigma_3$. In that point, J_2 can be expressed as a function of the Mohr-Coulomb friction angle $\phi_{MC} = \arctan(\mu_{MC})$ as

$$J_2 = \frac{4I_1^2 \sin^2(\phi_{MC})}{3[3 - \sin(\phi_{MC})]^2}, \quad (\text{B6})$$

so that, since $0 \leq \mu_{MC} \leq +\infty$, $0 \leq J_2/I_1^2 \leq 1/3$, and consequently, $3 \leq C_{DP} \leq +\infty$. From Eqs. (6), C_{DP} can be expanded as

$$\frac{C_{DP}}{3} = 1 + 3\mathcal{X} \left[1 + \frac{3}{4}(A_2\gamma_c) \frac{\pi - 8}{\sqrt{\pi}} \right] + O(A_2^3\gamma_c^3), \quad (\text{B7})$$

where we introduce the combination

$$\mathcal{X} = \frac{(I_1 - P_0)\pi^{3/2}S_1^2}{P_0^2[3S_0 + (3 + 4\sqrt{\pi})S_1]}, \quad (\text{B8})$$

which appears in all the following expansion. \mathcal{X} is all the smaller that ΔP is, and is constant in a given deviatoric plane. From Eq. (B7), we can check that C_{DP} does converge toward $1/3$ when $A_2\gamma_c$ is small, and becomes typically bigger than $1/3$ when $A_2\gamma_c$ grows.

A similar analysis can be performed in the cases of the Matsuoka-Nakai and Lade-Duncan criteria. First, notice that the ratio of tangential and normal stresses on the spatially mobilized plane is given by

$$\mu_{MN}^2 = \frac{C_{MN}}{9} - 1, \quad (\text{B9})$$

which holds independently of the precision of the Matsuoka-Nakai criterion (μ_{MN} is simply more or less constant). Since this ratio is positive by definition, $9 \leq C_{MN} \leq +\infty$. The expansion of this coefficient in the limit $A_2\gamma_c \ll 1$ is given by

$$\frac{C_{MN}}{9} = 1 + 6\mathcal{X} \left[1 + \frac{3}{4}(A_2\gamma_c) \frac{P_0(\pi - 8) + 6\pi S_1}{P_0\sqrt{\pi}} \right] + O(A_2^3\gamma_c^3). \quad (\text{B10})$$

Again, this is consistent with the known limiting behavior of this coefficient. Note also that in the limit where the hydrostatic pressure dominates the intrinsic strength of the material

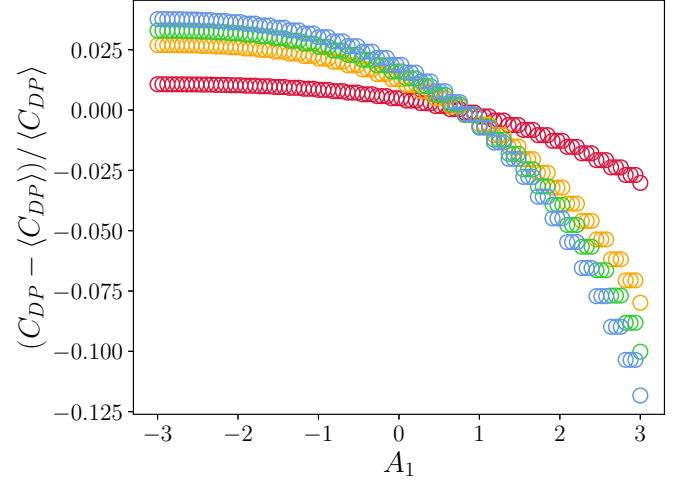


FIG. 5. Relative variation of the Drucker-Prager constant for various values of ΔP . The parameters are $S_0 = S_1 = 1$, $P_0 = 1$, $\gamma_c = 0.4$, $\Delta P = 0.05$ (red), $\Delta P = 0.5$ (orange), $\Delta P = 1$ (green), and $\Delta P = 2$ (blue).

$P_0 \gg S_1$, the second term in the bracket becomes similar to that of Eq. (B7).

Finally, using $C_{LD} = C_{MN}C_{DP}$, $27 \leq C_{LD} \leq +\infty$ [51]. The expansion of this coefficient in the limit $A_2\gamma_c \ll 1$ is given by

$$\frac{C_{LD}}{27} = 1 + 9\mathcal{X} \left[1 + \frac{3}{4}(A_2\gamma_c) \frac{P_0(\pi - 8) + 4\pi S_1}{P_0\sqrt{\pi}} \right] + O(A_2^3\gamma_c^3), \quad (\text{B11})$$

which is consistent with the boundaries.

APPENDIX C: ANALYSIS OF THE USUAL YIELD CRITERIA

Most yield criteria can be represented by a certain combination of invariants of the stress tensor being constant. This type of assertion is easy to test within the realm of our toy model. For a given yield criteria of equation $f_x(I_1, I_2, I_3) = C_x$, where C_x is a constant, we can evaluate f_x on a given deviatoric plane (in most cases, models are tested for a given value of I_1), compute its average on the whole yield surface cut in that plane, $\langle f_x \rangle$, and look at the relative variation $(f_x - \langle f_x \rangle)/\langle f_x \rangle$. Finally, in a given cut of the yield surface along a deviatoric plane, the data can be represented as a function of the Lode angle, or equivalently as a function of the parameter A_1 of our surface parametrization. In this way, we get the Figs. 5, 6 and 7.

More precisely, the determination of I_1 , I_2 , and I_3 depend on P_0 , which is fixed by the environment and thus not prescribed in our model. As can be expected, as P_0 becomes larger and larger compared to the values of the intrinsic stress scales S_0 and S_1 , the approximation of C_{LD} and C_{MN} by constant values is of better and better quality.

1. Effective friction coefficient

The effective friction coefficient is defined as a function of the total pressure $P = P_0 + \Delta P$. However, there is no prescription for P_0 in our formalism. The evolution of effective

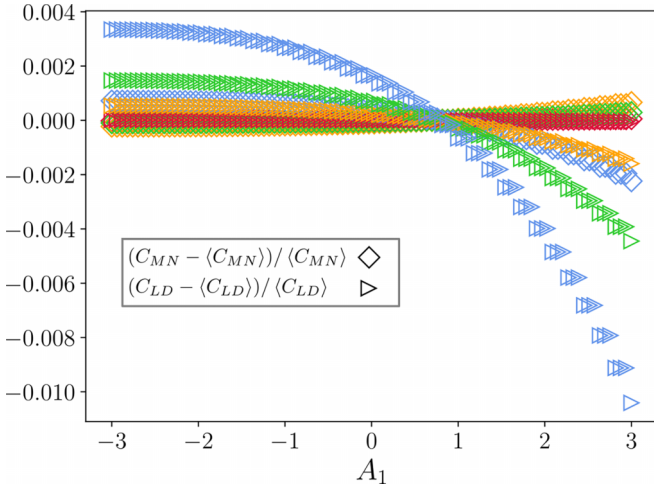


FIG. 6. Relative variation of the Matsuoka-Nakai (diamond) and Lade-Duncan (triangles) constants for various values of ΔP . The parameters are $S_0 = S_1 = 1$, $P_0 = 1$, $\gamma_c = 0.4$, $\Delta P = 0.05$ (red), $\Delta P = 0.42$ (orange), $\Delta P = 1$ (green), and $\Delta P = 2$ (blue).

friction can still be observed through the study of the reduced friction $\Delta\mu = \sigma_0/\Delta P$. Its evolution as a function of the Lode angle (represented by A_1) for various values of ΔP is displayed in Fig. 8, while Fig. 9 represents its relative variations.

While looking at Fig. 8, it should be kept in mind that what we represent is only the reduced friction coefficient and not the total one. Therefore, relatively large values of $\Delta\mu$ must not be deemed too surprising, they are reduced by the total confining pressure P_0 .

We chose to represent $\Delta\mu$ for both definitions of the shear stress σ_0 , from the solid and the liquid stress tensors, respectively, to illustrate the very close proximity of the predictions in both frameworks. Indeed, this difference appears to be visible only for its relative variation, and only for the largest values of ΔP (in units of S_0, S_1).

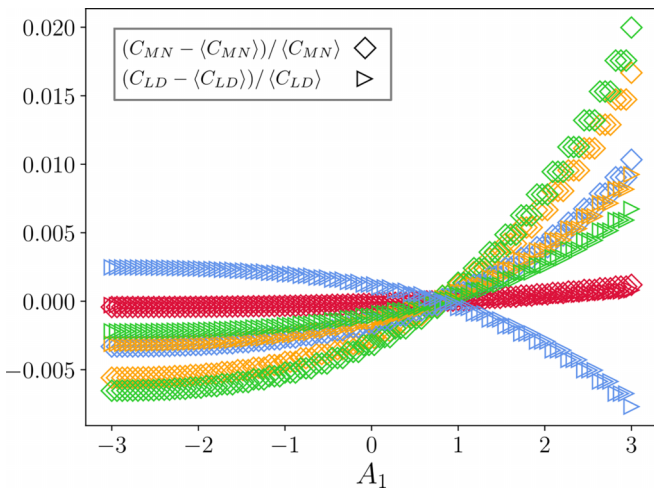


FIG. 7. Relative variation of the Matsuoka-Nakai (diamonds) and Lade-Duncan (triangles) constants for various values of ΔP . The parameters are $S_0 = S_1 = 1$, $P_0 = 0.5$, $\gamma_c = 0.4$, $\Delta P = 0.05$ (red), $\Delta P = 0.5$ (orange), $\Delta P = 1$ (green), and $\Delta P = 2$ (blue).

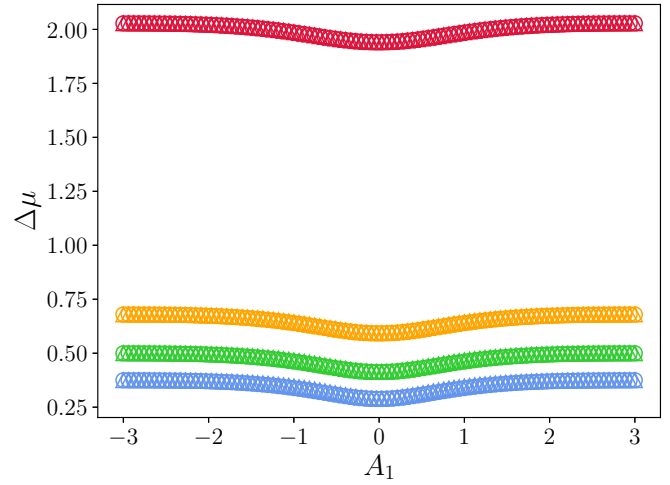


FIG. 8. Evolution of $\Delta\mu = \sigma_0/\Delta P$ as a function of A_1 for $\sigma_0 = \sigma_0^s$ (triangles) and $\sigma_0 = \sigma_0^l$ (circles). The parameters are $S_0 = S_1 = 1$, $\gamma_c = 0.4$, $\Delta P = 0.05$ (red), $\Delta P = 0.5$ (orange), $\Delta P = 1$ (green), and $\Delta P = 2$ (blue).

Then, we can study the variation of the effective friction coefficients as prescribed by the Matsuoka-Nakai and Lade-Duncan criteria, and corresponding to definition 2 of the effective friction coefficient. The relations between μ_{MN} (or μ_{LD}) and C_{MN} (or C_{LD}) can be found in [51]. Doing so requires to choose a value of P_0 . Results for a sample of values are shown on Figs. 10, 11 and 12. It should be kept in mind that comparing the precision to that of the toy-model of this figure makes no sense since Fig. 9 presents only the reduced friction coefficient $\Delta\mu$ which necessarily varies more than μ .

As for the case of the effective friction from the toy model, at least for high-enough value of P_0 , the effective friction is not constant in a given deviatoric plane, and even more so that ΔP is large (or equivalently, that the yield surface cut's shape becomes more and more triangular). At high values of

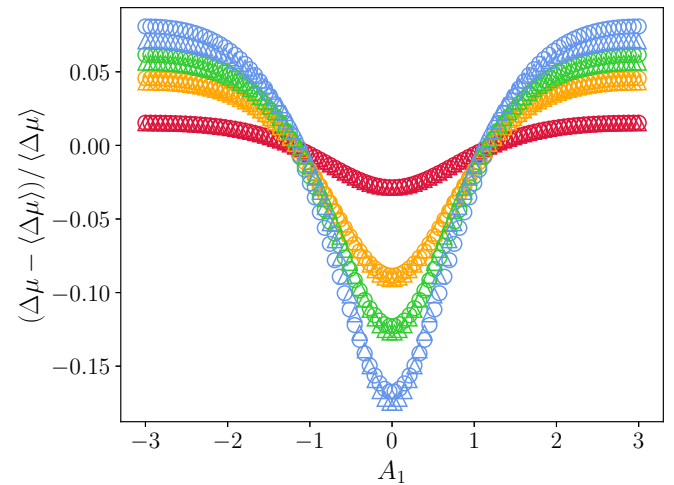


FIG. 9. Evolution of the relative variation of $\Delta\mu = \sigma_0/\Delta P$ as a function of A_1 for $\sigma_0 = \sigma_0^s$ (triangles) and $\sigma_0 = \sigma_0^l$ (circles). The parameters are $S_0 = S_1 = 1$, $\gamma_c = 0.4$, $\Delta P = 0.05$ (red), $\Delta P = 0.5$ (orange), $\Delta P = 1$ (green), and $\Delta P = 2$ (blue).

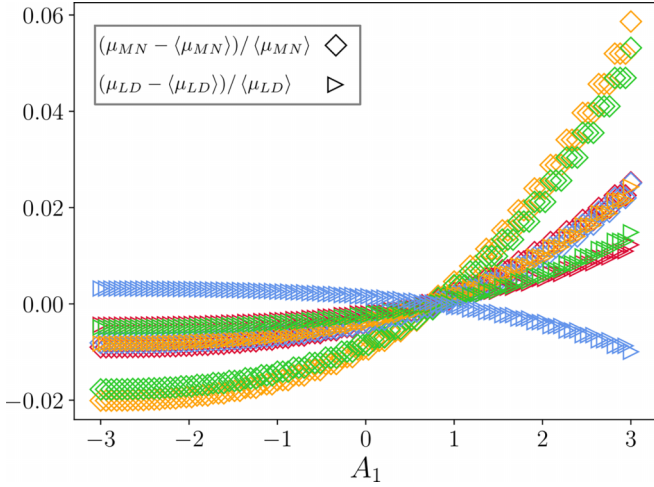


FIG. 10. Relative variation of the Matsuoka-Nakai (diamonds) and Lade-Duncan (triangles) effective friction coefficients for various values of ΔP . The parameters are $S_0 = S_1 = 1$, $P_0 = 0.5$, $\gamma_c = 0.4$, $\Delta P = 0.05$ (red), $\Delta P = 0.5$ (orange), $\Delta P = 1$ (green), and $\Delta P = 2$ (blue).

P_0 , both effective friction coefficient variations collapse onto each other. Perhaps more surprising, it seems to be an optimal value of mild P_0 where the variations are reduced at best.

APPENDIX D: IDENTIFICATION OF THE STRAIN TENSOR

To get a deeper understanding of the physical content of our toy model, let us push it a bit further and replace the screening factor with a Heaviside function $\Theta(1 - \dot{\gamma}t/\gamma_c)$. Moreover, since we mainly study the high Weissenberg number regime $Wi \gg 1$, the decay of the structural relaxation term $\exp(-\Gamma t)$ happens outside of the Heaviside window, our dynamical ansatz reduces to $\Phi_{q(t)}(t) \simeq \Theta(1 - \dot{\gamma}t/\gamma_c)$.

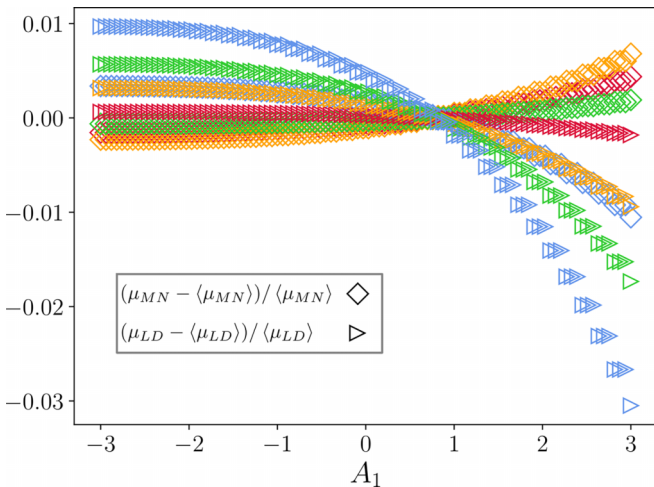


FIG. 11. Relative variation of the Matsuoka-Nakai (diamonds) and Lade-Duncan (triangles) effective friction coefficients for various values of ΔP . The parameters are $S_0 = S_1 = 1$, $P_0 = 1$, $\gamma_c = 0.4$, $\Delta P = 0.05$ (red), $\Delta P = 0.5$ (orange), $\Delta P = 1$ (green), and $\Delta P = 2$ (blue).

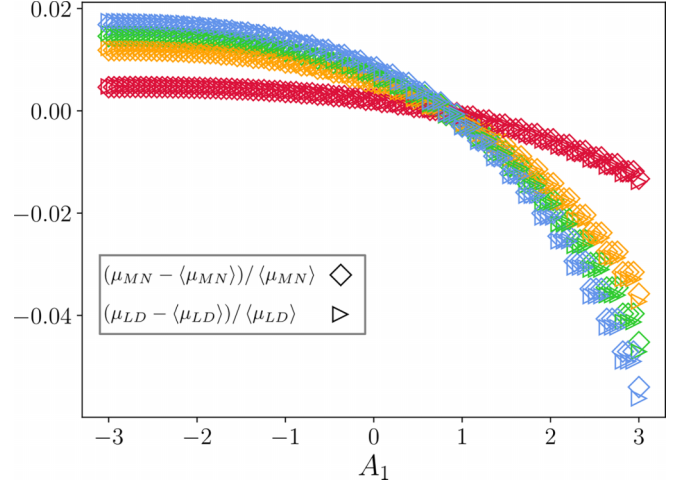


FIG. 12. Relative variation of the Matsuoka-Nakai (diamonds) and Lade-Duncan (triangles) effective friction coefficients for various values of ΔP . The parameters are $S_0 = S_1 = 1$, $P_0 = 10$, $\gamma_c = 0.4$, $\Delta P = 0.05$ (red), $\Delta P = 0.5$ (orange), $\Delta P = 1$ (green), and $\Delta P = 2$ (blue).

Then, using Eqs. (A11) and the results of the corresponding Appendix, and the fact that the flow is incompressible, the correction to the j th component of the stress tensor is given by

$$\begin{aligned} \Delta\sigma_{jj} &\simeq 2S_1\bar{\kappa}_{jj} \int_0^{+\infty} \dot{\gamma} dt \exp(2\bar{\kappa}_{jj}\dot{\gamma}t)\Theta(1 - \dot{\gamma}t/\gamma_c)^2 \\ &= S_1 [\exp(2\bar{\kappa}_{jj}\gamma_c) - 1]. \end{aligned} \quad (\text{D1})$$

Let us have a close look at the term inside the brackets. The first term has a form of a Finger tensor for a strain given by the typical strain scale γ_c , and the strength of the flow from which the strain originates, $\bar{\kappa}_{jj}$. The term inside the brackets can therefore be understood as the difference between the metric in the deformed state, and the unit metric, which is by definition the strain tensor (or more precisely here its j th component). Equation (D1) can thus be straightforwardly read as a Hooke's law, with a shear modulus S_1 and a strain tensor $\exp(2\bar{\kappa}_{jj}\gamma_c) - 1$.

The incompressibility condition $\text{Tr}(\kappa) = 0$ ensures that the determinant of the deformation tensor is equal to 1, or here that the determinant of the Finger tensor is 1. In the limit of small deformations, which corresponds to $\bar{\kappa}_{jj}\gamma_c \ll 1$ (or more precisely, $A_2\gamma_c \ll 1$, see the Appendix on the Drucker-Prager limit) one recovers the well-known result that ϵ is fully deviatoric [$\text{Tr}(\epsilon) = 0$]. However, pay attention to the fact that this result only holds in this limit.

This model is, of course, too simple to be really accurate, but it shows how ϵ can be identified in our set of equations. When the Heaviside profile is replaced by the Gaussian one used in the paper, the procedure stays the same, although the results are less obvious to interpret since ϵ is now expressed as a function of \mathcal{F} , which does not let the difference between the strained and unstrained metrics appear explicitly. As it turns out, going from the sharp Heaviside profile to the smoother Gaussian one amounts to accounting for the

fact that advection is not an instantaneous process, and as a result, the final expression of the strain is smoothed. The use of a Lorentzian profile, such as the one used in [60] would

probably lead to the identification of the same type of function, although in that case, the integral cannot be performed exactly.

-
- [1] J. Lin, E. Lerner, A. Rosso, and M. Wyart, *Proc. Natl. Acad. Sci. USA* **111**, 14382 (2014).
- [2] J. Lin, T. Gueudré, A. Rosso, and M. Wyart, *Phys. Rev. Lett.* **115**, 168001 (2015).
- [3] I. Fernández Aguirre and E. A. Jagla, *Phys. Rev. E* **98**, 013002 (2018).
- [4] C. Liu, E. E. Ferrero, K. Martens, and J.-L. Barrat, *Soft Matter* **14**, 8306 (2018).
- [5] A. Nicolas, E. E. Ferrero, K. Martens, and J.-L. Barrat, *Rev. Mod. Phys.* **90**, 045006 (2018).
- [6] E. E. Ferrero and E. A. Jagla, *Phys. Rev. Lett.* **123**, 218002 (2019).
- [7] A. Wisitsorasak and P. G. Wolynes, *Proc. Natl. Acad. Sci. USA* **109**, 16068 (2012).
- [8] S. K. Nandi, G. Biroli, J.-P. Bouchaud, K. Miyazaki, and D. R. Reichman, *Phys. Rev. Lett.* **113**, 245701 (2014).
- [9] R. Dasgupta, H. G. E. Hentschel, and I. Procaccia, *Phys. Rev. Lett.* **109**, 255502 (2012).
- [10] R. Dasgupta, H. G. E. Hentschel, and I. Procaccia, *Phys. Rev. E* **87**, 022810 (2013).
- [11] M. Moshe, E. Sharon, and R. Kupferman, *Phys. Rev. E* **92**, 062403 (2015).
- [12] E. DeGiuli, *Phys. Rev. E* **98**, 033001 (2018).
- [13] E. DeGiuli, *Phys. Rev. Lett.* **121**, 118001 (2018).
- [14] E. DeGiuli, *Phys. Rev. E* **101**, 043002 (2020).
- [15] A. Lemaître, C. Mondal, M. Moshe, I. Procaccia, S. Roy, and K. Screiber-Re'em, *Phys. Rev. E* **104**, 024904 (2021).
- [16] S. M. Fielding, P. Sollich, and M. E. Cates, *J. Rheol.* **44**, 323 (2000).
- [17] M. J. Alava, P. K. V. V. Nukala, and S. Zapperi, *Adv. Phys.* **55**, 349 (2006).
- [18] E. Bouchbinder, T. Goldman, and J. Fineberg, *Rep. Prog. Phys.* **77**, 046501 (2014).
- [19] C. Rainone, P. Urbani, H. Yoshino, and F. Zamponi, *Phys. Rev. Lett.* **114**, 015701 (2015).
- [20] P. K. Jaiswal, I. Procaccia, C. Rainone, and M. Singh, *Phys. Rev. Lett.* **116**, 085501 (2016).
- [21] G. Parisi, I. Procaccia, C. Rainone, and M. Singh, *Proc. Natl. Acad. Sci. USA* **114**, 5577 (2017).
- [22] P. Urbani and F. Zamponi, *Phys. Rev. Lett.* **118**, 038001 (2017).
- [23] M. Popović, T. W. J. de Geus, and M. Wyart, *Phys. Rev. E* **98**, 040901(R) (2018).
- [24] M. Ozawa, L. Berthier, G. Biroli, A. Rosso, and G. Tarjus, *Proc. Natl. Acad. Sci. USA* **115**, 6656 (2018).
- [25] M. Ozawa, L. Berthier, G. Biroli, and G. Tarjus, *Phys. Rev. Res.* **2**, 023203 (2020).
- [26] M. L. Goff, E. Bertin, and K. Martens, *J. Phys. Mater.* **3**, 025010 (2020).
- [27] H. J. Barlow, J. O. Cochran, and S. M. Fielding, *Phys. Rev. Lett.* **125**, 168003 (2020).
- [28] C. Ancey, *J. Nonnewton. Fluid Mech.* **142**, 4 (2007).
- [29] M. Huang, X. Lu, and J. Qian, *Int. J. Numer. Anal. Methods Geomech.* **34**, 906 (2010).
- [30] M. Mehranpour and P. Kulatilake, *Geomech. Geophys. Geoenerg. Geo-resour.* **2**, 203 (2016).
- [31] F. Radjai, J.-N. Roux, and A. Daouadjji, *J. Eng. Mech.* **143**, 04017002 (2017).
- [32] F. Zeng, Y. Li, and J. F. Labuz, *J. Geotech. Geoenviron. Eng.* **144**, 06017018 (2018).
- [33] J. Fei, Y. Jie, X. Sun, and H. Xiong, *Sci. Rep.* **10**, 12162 (2020).
- [34] A. Singh, R. Ayothiraman, and K. Rao, *Geotech. Geol. Eng.* **38**, 4385 (2020).
- [35] S. Wang, H. Masoumi, J. Oh, and S. Zhang, *Scale-Size and Structural Effects of Rock Materials* (Tsinghua University Press, Elsevier, 2020).
- [36] M. François, *C. R. Mec.* **336**, 417 (2008).
- [37] J. Zhang, Z. Zhang, and C. Chen, *Acta Mech. Solida Sin.* **23**, 220 (2010).
- [38] J. Pan, C. Zhang, Y. Xu, and F. Jin, in *Seismic Safety Evaluation of Concrete Dams*, edited by C. Zhang, F. Jin, J. Wang, and Y. Xu (Butterworth-Heinemann, Oxford, 2013), pp. 283–310.
- [39] J.-F. Jiang and Y.-F. Wu, *J. Eng. Mech.* **140**, 04014096 (2014).
- [40] S. Abrate, *J. Sandw. Struct. Mater.* **10**, 5 (2008).
- [41] D. Drucker and W. Prager, *Q. Appl. Math.* **10**, 157 (1952).
- [42] B. Paul, *Int. J. Solids Struct.* **4**, 175 (1968).
- [43] P. Lade and J. Duncan, *J. Geotech. Eng. Div.* **101**, 1037 (1975).
- [44] J. Goddard, *J. Nonnewton. Fluid Mech.* **14**, 141 (1984).
- [45] H. Matsuoka and T. Nakai, *Soils Found.* **25**, 123 (1985).
- [46] P. Brunn and H. Asoud, *Rheol. Acta* **41**, 524 (2002).
- [47] D. Bigoni and A. Piccolroaz, *Int. J. Solids Struct.* **41**, 2855 (2004).
- [48] H. Matsuoka and D. Sun, *The SMP Concept-Based 3D Constitutive Models for Geomaterials* (Taylor and Francis Group, London, 2006).
- [49] J. Labuz and A. Zang, *Rock Mech. Rock Eng.* **45**, 975 (2012).
- [50] R. Lagioia and A. Panteghini, *Proc. R. Soc. A* **472**, 20150713 (2016).
- [51] J. Fleischmann, *Geotech. Geol. Eng.* **38**, 5409 (2020).
- [52] E. Clouet, B. Bienvenu, L. Dezerald, and D. Rodney, *C. R. Phys.* **22**, 83 (2021).
- [53] W. T. Kranz, M. Sperl, and A. Zippelius, *Phys. Rev. Lett.* **104**, 225701 (2010).
- [54] W. T. Kranz, M. Sperl, and A. Zippelius, *Phys. Rev. E* **87**, 022207 (2013).
- [55] W. T. Kranz, F. Frahsa, A. Zippelius, M. Fuchs, and M. Sperl, *Phys. Rev. Lett.* **121**, 148002 (2018).
- [56] W. T. Kranz, F. Frahsa, A. Zippelius, M. Fuchs, and M. Sperl, *Phys. Rev. Fluids* **5**, 024305 (2020).
- [57] O. Coquand, M. Sperl, and W. T. Kranz, *Phys. Rev. E* **102**, 032602 (2020).
- [58] O. Coquand, W. T. Kranz, and M. Sperl, *arXiv:2008.05931*.
- [59] O. Coquand and M. Sperl, *Phys. Rev. E* **104**, 014604 (2021).
- [60] J. Brader, T. Voigtman, M. Fuchs, R. Larson, and M. Cates, *Proc. Natl. Acad. Sci. USA* **106**, 15186 (2009).
- [61] Other yield criteria, used primarily to describe the failure of metals, such as the Von-Mises' criterion are not discussed here.

- Indeed, they can be directly deduced from the ones we present by neglecting the dependence in the pressure invariant I_1 .
- [62] Indeed, if we define an internal friction angle α by $\mu_{MC} = \tan(\alpha)$, we can show that the ratio of the length d_0 between the hydrostatic axis $\sigma_1 = \sigma_2 = \sigma_3$ and the point of the Lode angle $\theta = 0$ and that of the Lode angle $\theta = \pi/3$ (both represented as big green dots on Fig. 1), d_{60} , is given by $d_0^2/d_{60}^2 = [3 + \sin(\alpha)]/[3 - \sin(\alpha)]$. Given that $\alpha \in [0; \pi/2]$ by definition, this ratio can be equal to 1 only if $\alpha = 0$, in which case $\mu = 0$ as well.
- [63] M. Fuchs and M. E. Cates, *Phys. Rev. Lett.* **89**, 248304 (2002).
- [64] M. Fuchs and M. Cates, *Farad. Disc.* **123**, 267 (2003).
- [65] M. Fuchs and M. Cates, *J. Rheol.* **53**, 957 (2009).
- [66] Indeed, there is no obvious expansion parameter in that case. Another way of generating polynomial equations is to approximate $\mathcal{F}(x)$ by a rational fraction, which gives pretty accurate results for the physical region of moderate values of x .
- [67] GDR MiDi, *Eur. Phys. J. E* **14**, 341 (2004).
- [68] F. da Cruz, S. Emam, M. Prochnow, J.-N. Roux, and F. Chevoir, *Phys. Rev. E* **72**, 021309 (2005).
- [69] P. Jop, Y. Forterre, and O. A. Pouliquen, *Nature (London)* **441**, 727 (2006).
- [70] C. Cassar, M. Nicolas, and O. Pouliquen, *Phys. Fluids* **17**, 103301 (2005).
- [71] F. Boyer, E. Guazzelli, and O. Pouliquen, *Phys. Rev. Lett.* **107**, 188301 (2011).
- [72] M. Houssais and D. J. Jerolmack, *Geomorphology* **277**, 251 (2017).
- [73] E. Guazzelli and O. Pouliquen, *J. Fluid Mech.* **852**, P1 (2018).
- [74] R. Larson and H. Brenner, *Constitutive Equations for Polymer Melts and Solutions: Butterworths Series in Chemical Engineering* (Elsevier Science, Boston, MA, 2013).
- [75] The very large ΔP regime is not explored. Indeed, in that case, the yield surface has sharper edges which are not so common in the experimental literature so that the relevance of this regime for real, physical systems is not obvious.